High performance GaSb based digital-grown InGaSb/AlGaAsSb mid-infrared lasers and bars

Sheng-Wen Xie(谢圣文), Yu Zhang(张宇), Cheng-Ao Yang(杨成奥), Shu-Shan Huang(黄书山), Ye Yuan(袁野), Yi Zhang(张一), Jin-Ming Shang(尚金铭), Fu-Hui Shao(邵福会), Ying-Qiang Xu(徐应强), Hai-Qiao Ni(倪海桥), Zhi-Chuan Niu(牛智川)

Citation: Chin. Phys. B . 2019, 28(1): 014208. **doi:** 10.1088/1674-1056/28/1/014208

Journal homepage: http://cpb.iphy.ac.cn; http://iopscience.iop.org/cpb

What follows is a list of articles you may be interested in

Room-temperature continuous-wave interband cascade laser emitting at 3.45 μm

Yi Zhang(张一), Fu-Hui Shao(邵福会), Cheng-Ao Yang(杨成奥), Sheng-Wen Xie(谢圣文), Shu-Shan Huang(黄书山), Ye Yuan(袁野), Jin-Ming Shang(尚金铭), Yu Zhang(张宇), Ying-Qiang Xu(徐应强), Hai-Qiao Ni(倪海桥), Zhi-Chuan Niu(牛智川)

Chin. Phys. B . 2018, 27(12): 124207. **doi:** 10.1088/1674-1056/27/12/124207

Semiconductor photonic crystal laser

Wanhua Zheng(郑婉华)

Chin. Phys. B . 2018, 27(11): 114211. **doi:** 10.1088/1674-1056/27/11/114211

Electrically pumped metallic and plasmonic nanolasers

Martin T Hill

Chin. Phys. B . 2018, 27(11): 114210. **doi:** 10.1088/1674-1056/27/11/114210

Surface plasmon polariton nanolasers: Coherent light sources for new applications

Yu-Hsun Chou(周昱薰), Chia-Jui Chang(張家睿), Tzy-Rong Lin(林資榕), Tien-Chang Lu(盧廷昌)

Chin. Phys. B . 2018, 27(11): 114208. **doi:** 10.1088/1674-1056/27/11/114208

Thermal analysis of GaN-based laser diode mini-array

Jun-Jie Hu(胡俊杰), Shu-Ming Zhang(张书明), De-Yao Li(李德尧), Feng Zhang(张峰), Mei-Xin Feng(冯美鑫), Peng-Yan Wen(温鹏雁), Jian-Pin Liu(刘建平), Li-Qun Zhang(张立群), Hui Yang(杨辉)

Chin. Phys. B . 2018, 27(9): 094208. **doi:** 10.1088/1674-1056/27/9/094208

Chin. Phys. B Vol. 28, No. 1 (2019) 014208

High performance GaSb based digital-grown InGaSb/AlGaAsSb mid-infrared lasers and bars*

Sheng-Wen Xie(谢圣文)[1,2], Yu Zhang(张宇)[1,2,†], Cheng-Ao Yang(杨成奥)[1,2], Shu-Shan Huang(黄书山)[1,2], Ye Yuan(袁野)[1,2], Yi Zhang(张一)[1,2], Jin-Ming Shang(尚金铭)[1,2], Fu-Hui Shao(邵福会)[1,2], Ying-Qiang Xu(徐应强)[1,2], Hai-Qiao Ni(倪海桥)[1,2], and Zhi-Chuan Niu(牛智川)[1,2,‡]

[1] *State Key Laboratory for Superlattices and Microstructures, Institute of Semiconductors, Chinese Academy of Sciences, Beijing* 100083, *China*

[2] *Center of Materials Science and Optoelectronics Engineering, University of Chinese Academy of Sciences, Beijing* 100049, *China*

(Received 27 August 2018; published online 12 December 2018)

InGaSb/AlGaAsSb double-quantum-well diode lasers emitting around 2 μm are demonstrated. The AlGaAsSb barriers of the lasers are grown with digital alloy techniques consisting of binary AlSb/AlAs/GaSb short-period pairs. Peak power conversion efficiency of 26% and an efficiency higher than 16% at 1 W are achieved at continuous-wave operation for a 2-mm-long and 100-μm-wide stripe laser. The maximum output power of a single emitter reaches to 1.4 W at 7 A. 19-emitter bars with maximum efficiency higher than 20% and maximum power of 16 W are fabricated. Lasers with the short-period-pair barriers are proved to have improved temperature properties and wavelength stabilities. The characteristic temperature (T_0) is up to 140 °C near room temperature (25–55 °C).

Keywords: mid-infrared laser diode, digital alloys, characteristic temperature, bars

PACS: 42.55.Px, 78.55.Cr, 78.67.De, 42.60.Pk **DOI:** 10.1088/1674-1056/28/1/014208

1. Introduction

GaSb based InGaSb/AlGaAsSb multi-quantum well structures are recognized as the most suitable structures for lasers emitting around 2 μm in terms of output power and power conversion efficiency (PCE).[1,2] However, the structure has serious flaws in the energy band design.[3] The valence band offset is no more than 0.1 eV even if between an $In_{0.4}Ga_{0.6}Sb$ well and an $Al_{0.25}Ga_{0.75}As_{0.02}Sb_{0.98}$ barrier, a limiting quantum well structure which actually may not be used in practice. With the increased In composition (InGaSb) in the well, however, the valence band offset becomes smaller. The poor offset means poor hole confinement, leading to increased thermionic emission of carriers from quantum wells, and the increased thermionic emission leads to an increase of the threshold current because of the leakage current, which would lead to poor device performance eventually.

Therefore, we involved digital alloys[4] as the barriers of active layers in the band design to increase the effective barrier height. Quantum well lasers with digital alloy as barriers have improved temperature stability, namely, higher characteristic temperature.[5] It is mainly attributed to the less thermionic emission of carriers because of the good carrier confinement.

In this article, we report results on diode lasers and bars emitting around 2 μm, part structure of which were grown with digital alloys. The AlGaAsSb barriers and gradient layers were digital alloys (DA), and the remaining structures including InGaSb wells were random alloys (RA).

2. Device design

The partial digital-grown lasers discussed in this paper were grown on Te-doped GaSb substrates by Gen-II molecular beam epitaxy (MBE) system. 500 nm Te-doped GaSb buffer was firstly grown after the deoxydation of the substrate, followed by 2000 nm N-type $Al_{0.5}Ga_{0.5}As_{0.04}Sb_{0.96}$ cladding layer. Two quantum wells were grown between 500 nm undoped $Al_{0.25}Ga_{0.75}As_{0.02}Sb_{0.98}$ waveguide layers. And the structure was ended with a 250 nm p^+ GaSb cap. Between the claddings of high Al component (0.5) and the waveguides of low Al component (0.25) were 39 nm gradient layers grown via digital alloy technique. The 20 nm $Al_{0.25}Ga_{0.75}As_{0.02}Sb_{0.98}$ barriers on both sides of the 9 nm InGaSb wells were designed to be digital alloys too.

The AlGaAsSb digital alloy barriers are grown with pairs of short superlattices of 3 nm as a cycle. One circle is grown with the sequence of AlSb (t_1)/AlAs (t_2)/AlSb (t_1)/GaSb (t_3). The total growth time ($2t_1+t_2+t_3$) of a circle is about 20 s. Digital alloys also bring benefits to the epitaxial growth.[6] The As vapor pressure is too low to be stable when growing lattice-matched $Al_{0.25}Ga_{0.75}As_{0.02}Sb_{0.98}$ barriers using traditional MBE technique. As a result, it is difficult to control the Sb/As ratio to grown perfectly lattice-matched crystals. However, the component of AlGaAsSb digital alloys is decided by

*Project supported by the National Natural Science Foundation of China (Grant Nos. 61790580 and 61435012), the National Basic Research Program of China (Grant No. 2014CB643903), and the Scientific Instrument Developing Project of the Chinese Academy of Sciences (Grant No. YJKYYQ20170032).

†Corresponding author. E-mail: zhangyu@semi.ac.cn

‡Corresponding author. E-mail: zcniu@semi.ac.cn

© 2019 Chinese Physical Society and IOP Publishing Ltd

the shutter time of the binary materials $((2t_1+t_2)/t_3)$ instead of the V group ratio, which perfectly solves the problem of instability of the As vapor pressure.

The schematic shutter sequences during the gradient layers growth from $Al_{0.5}Ga_{0.5}As_{0.04}Sb_{0.96}$ to $Al_{0.25}Ga_{0.75}As_{0.02}Sb_{0.98}$ are shown in Fig. 1. Figure 2 depicts the energy-band structures of the broadened-waveguide InGaSb (RA)/AlGaAsSb (DA) double-quantum-well laser. The wafer then was processed into 2-mm-long, 100-μm-wide stripe chips with standard contact optical lithography in combination with etching process.[7] 250 nm SiO_2 was deposited to be used as insulation after the 2 μm ridge was etched. The wafer was thinned to 130 nm. 50 nm/50 nm/300 nm Ti/Pt/Au and 50 nm/50 nm/300 nm-1000 nm AuGeNi-Au were used as P-contact metals and N-contact metals respectively deposited by thermal evaporation equipment. Then the wafer was cleaved into bars and chips. The chip facets were high (> 95%)/anti (< 5%)-reflection coated targeting the lasing wavelength, and the devices were indium-soldered p-side down on C-mount heatsinks and characterized. The bars including 19 single HR/AR coated emitters were mounted on CS heatsinks and characterized.

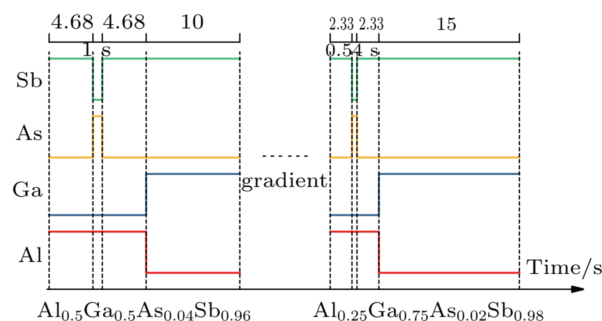

Fig. 1. Schematic time shutter sequence utilized during gradient layers growth from $Al_{0.5}Ga_{0.5}As_{0.04}Sb_{0.96}$ to $Al_{0.25}Ga_{0.75}As_{0.02}Sb_{0.98}$ via digital alloy technique.

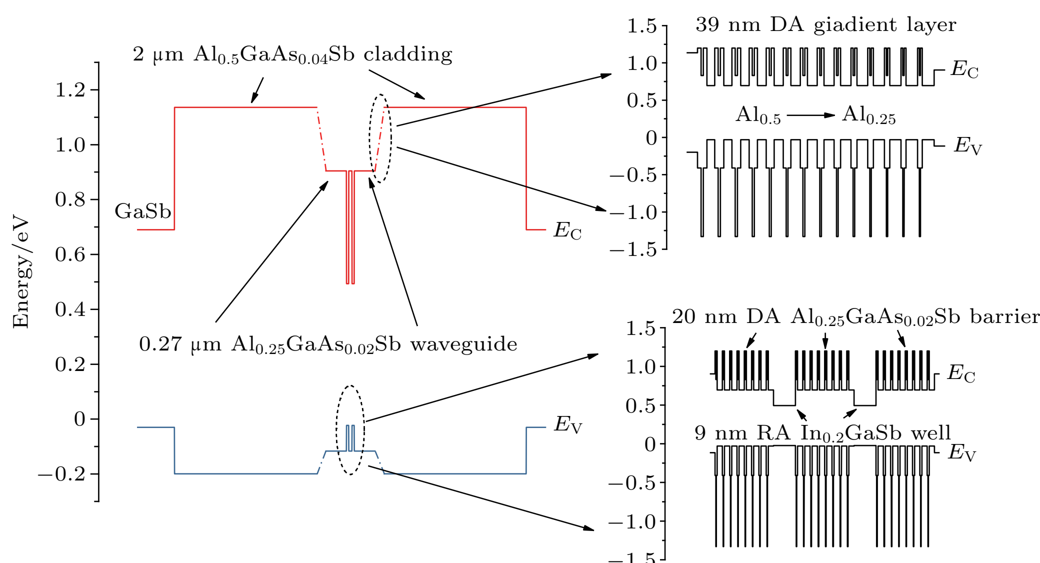

Fig. 2. Schematic energy-band diagram of the broadened-waveguide diode laser. The insets show the energy band of digital alloys varying from $Al_{0.5}Ga_{0.5}As_{0.04}Sb_{0.96}$ to $Al_{0.25}Ga_{0.75}As_{0.02}Sb_{0.98}$ and the energy band of InGaSb (RA)/$Al_{0.25}Ga_{0.75}As_{0.02}Sb_{0.98}$ (DA) quantum wells.

3. Results

The power conversion efficiency η is a significant parameter to characterize the overall performance[8] of a diode laser, which is defined as $\eta = P_{out}/(IV)$, where P_{out} is the output power, and I and V are the operating current and voltage. The power conversion efficiency along with the optical output power versus the injection current of our partial digital-grown laser is plotted in Fig. 3. The measurement for the single 2000 μm×100 μm laser was performed under TEC-cooling at 290 K. In the extrapolation of the I–V characteristic back to $I = 0$, the laser turn-on voltage $V_0 = 0.672$ V is obtained. One of the empirical terms reducing PCE is the voltage waste, which is a combination of the voltage drop of junction interface and electrical resistance. The turn-on voltage 0.672 V is basically the same as the photon energy, which means that the short period superlattices (digital alloys) do not increase the voltage wastes in consideration of the voltage drop between the waveguides and cladding layers. The measured maximum power is 1.4 W at 7 A under continuous-wave (CW) operation with PCE higher than 10%. The low calculated series resistance of 158 mΩ results in the maximum efficiency 27% at 0.7 A. And higher than 15% PCE at 1 W output is achieved, which is remarkable for lasers emitting around 2 μm.[9,10] Another remarkable characteristic of the partial digital-grown emitter is the threshold current density (J_{th}), which is as low as 52 A/cm^2. Judging from the output power and efficiency of a diode laser, the partial digital-grown laser is no worse than that without digital alloys.[2,10]

Many studies have focused on diode lasers with digital alloy structures for their advantages of improving the device

temperature properties (high T_0).[11] However, most of them focused on the 1.3–1.5 μm wavelength range[12,13] and we have not found any research on this technique involving mid-infrared lasers emitting around 2 μm. To make it clear, lasers without digital alloy but had the same structures with the lasers described in this paper were fabricated for comparison. Figure 4 shows the threshold current density ($\ln(J_{th})$) in pulse operation versus heatsink temperature (25–95 °C) for a partial digital-grown InGaSb/AlGaAsSb quantum well laser (type A). The inset shows the temperature characteristic of an InGaSb/AlGaAsSb quantum well laser without digital alloy in its structures (type B). The stripe width and cavity length of type A and type B are the same, both 100 μm and 2 mm, respectively.

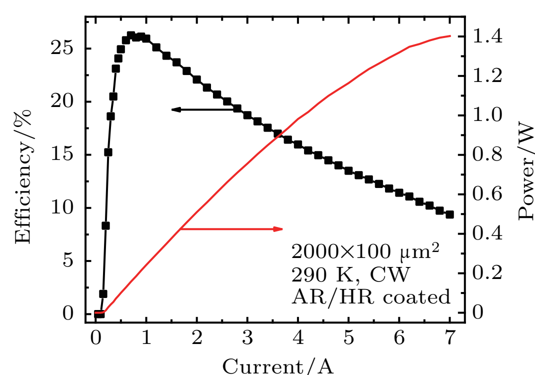

Fig. 3. Output power and power efficiency versus laser current for a 2000 μm×100 μm single emitter emitting around 2 μm. The facets were AR/HR coated and the device was mounted p-side down. Maximum CW power and power efficiency were 1.4 W and 26%, respectively.

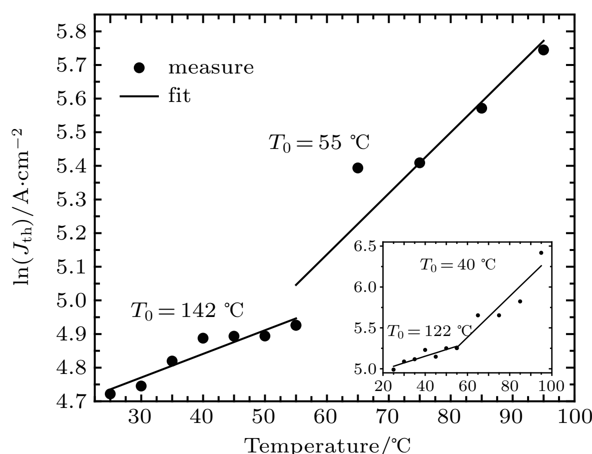

Fig. 4. Threshold current density versus heatsink temperature (25–95 °C) for a partial digital-grown InGaSb/AlGaAsSb quantum well laser. The inset shows the temperature characteristic of an InGaSb/AlGaAsSb quantum well laser without digital alloy in its structure.

The equation $J_{th} = J_0 \exp(T/T_0)$ is used to calculate the characteristic temperature T_0. Near room temperature (25–55 °C), the characteristic temperature T_0 for type A is 142 °C, compared with 122 °C for type B. At a temperature higher than 55 °C, the T_0 for type A decreases to 55 °C and for type B decreases to 40 °C. The decrease in T_0 for both types is mainly due to the increase in Auger recombination and current leakage with increasing temperature.

By comparison, the characteristic temperature T_0 of type A is larger than that of type B. Thus, we come to a conclusion that a laser with AlGaAsSb digital-alloy barriers has higher T_0 than that with AlGaAsSb random-alloy barriers. In conclusion, the short-period superlattices could also raise lasers' temperature properties at 2 μm wavelength range. The improvement in T_0 is attributed to the reduced thermionic emission of carriers out of the quantum wells because of the increased barrier height after using digital alloys as barriers.

For a given diode laser device, the wavelength increases with the operating current because of the chip core area temperature rise and the gap decrease in the InGaSb band. The normalized lasing spectra at different currents of a partial digital-grown laser at CW operation with natural heat dissipation are shown in Fig. 5. The inset shows the linear relationship between the lasing wavelengths and operating currents of the laser. Most electroluminescence measurements in Fig. 5 were performed on the Bruker Fourier transform infrared spectrometer with TE-InGaAs detector and the spectrum at 0.35 A with full-width at half-maximum (FWHM) only 1.8 nm was measured by Yokogawa OSA equipment with better accuracy.

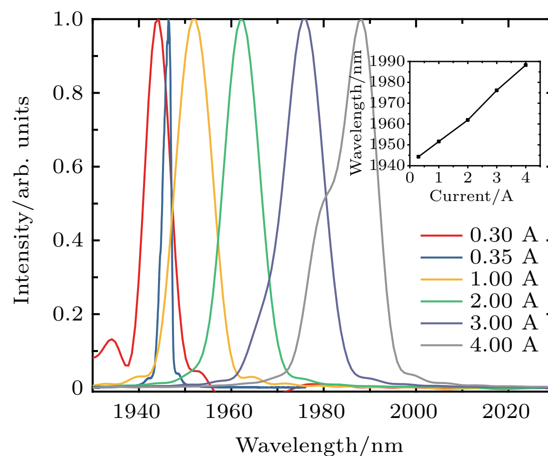

Fig. 5. Emission wavelengths at different injection currents for the partial digital-grown device at 290 K. The inset shows the relationship between lasing wavelengths and operating currents.

From the data, the emission wavelength shifts from 1951.62 nm to 1988.29 nm with the injection current increased from 1 A to 4 A because of the drifting of the gain peak. The slope is estimated to be 10 nm/A when the current is lower than 2 A. The slope increases to 13 nm/A after 2 A due to the thermal influence on mode selection, and the emitting spectra of a laser device without digital alloys were also measured and the red shift slope was about 20.14 nm/A which was two times as much as that of a partial digital-grown laser. The significant reduction in red shift slope for the partial digital-grown laser, which has not been mentioned in any paper before, may be attributed to the difference of thermal effect for digital alloys

and random alloys. The difference of thermal expansion coefficient between digital alloy barriers and random alloy barriers would cause different lattice mismatch between InGaSb wells and AlGaAsSb barriers. The different thermal conductivities of the two alloys might also be one of the causes.

High performance laser bars were also fabricated. Figure 6 shows the optical power for a 0.95 cm laser bar with 20% fill factor under CW operation. The bar contains 19 emitters including digital alloy as barriers and gradient layers in its structures, and is mounted on a CS heatsink. A peak power of 16 W is achieved at 70 A with water cooling systems at 290 K. The maximum power efficiency is higher than 26%, which is almost equal to that of a single emitter and higher than 20% efficiency is reached at 11 W, meeting the requirements of commercial product considerations.[14] The high performance of the 19-emitter-bar is a good proof that the optimization of the growth technique does not sacrifice the infrared laser performance and also a good proof of emitter uniformity around the whole wafer.[15]

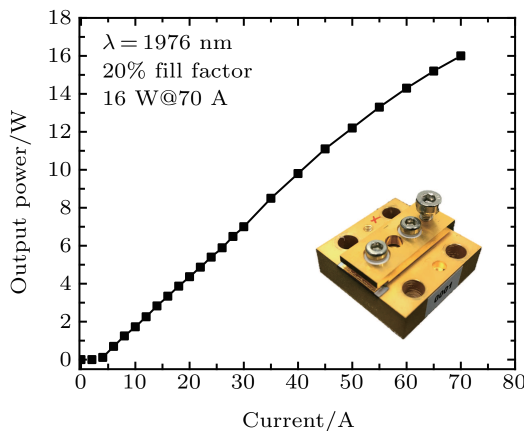

Fig. 6. Output power of a 0.95 cm diode laser bar emitting at 1976 nm.

4. Conclusion

In summary, we have investigated the influence of the digital alloys in diode laser emitting around 2 μm. By using digital alloys as the barriers and gradient layers in laser structures, an improved temperature property (higher T_0) is achieved, which is 142 °C near room temperature. It is also proved that the laser has better wavelength stability by comparison with lasers without digital alloys. The maximum power 1.4 W and the maximum efficiency 27% under CW operation are obtained from a single partial digital-grown emitter, which is a good result at present. A peak power of 16 W is also achieved at 70 A with a high performance 19-emitter-bar.

References

[1] Scholle K, Lamrini S, Koopmann P and Fuhrberg P 2010 *2 μm Laser Sources and Their Possible Applications*
[2] Peters M, Rossin V, Everett M, *et al.* 2007 *Proc. SPIE* 6456
[3] Peters M, Rossin V and Zucker E 2007 *High-Power Diode Laser Technology and Applications V* p. 1217
[4] Lyu Y, Han X, Sun Y, Jiang Z, Guo C, Xiang W, Dong Y, Cui J, Yao Y, Jiang D, Wang G, Xu Y and Niu Z 2018 *J. Cryst. Growth* **482** 70
[5] Schafer F, Mayer B, Reithmaier J P and Forchel A 1998 *Appl. Phys. Lett.* **73** 2863
[6] Mourad C, Gianardi D, Malloy K J and Kaspi R 2000 *J. Appl. Phys.* **88** 5543
[7] Yang C, Zhang Y, Liao Y, Xing J, Wei S, Zhang L, Xu Y, Ni H and Niu Z 2016 *Chin. Phys. B* **25** 24204
[8] Li H, Chyr I, Srinivasan R, *et al.* 2007 *Proc. of SPIE* **6456** 64560C
[9] Shterengas L, Belenky G, Kisin M V and Donetsky D 2007 *Appl. Phys. Lett.* **90** 11119
[10] Chen J, Kipshidze G and Shterengas L 2010 *IEEE J. Quantum Electron.* **46** 1464
[11] Postigo P A, Golmayo D, Gomez H, Rodriguez D and Dotor M L 2002 *Jpn. J. Appl. Phys. Pt Lett.* **41** L565
[12] Liu G T, Stintz A, Pease E A and Newell T C 2000 *Photon. Technol. Lett. IEEE* **12** 4
[13] Heo D, Song J D, Han I K, Choi W J and Yong T L 2013 *IEEE J. Quantum Electron.* **49** 24
[14] Stickley C M and Hach E E 2006 *Proc. of SPIE* **6104** 610405
[15] Kelemen M T, Rattunde M and Wagner J 2010 *Proc. SPIE* **7583** 75830O